UDC 539.4

Disturbance Due to Thermomechanical Sources in Porothermoelastic Medium

R. Kumar[a,1] and I. A. Abbas[b,c,2]

[a] Department of Mathematics, Kurukshetra University, Kurukshetra, Haryana, India

[b] Department of Mathematics, Faculty of Science and Arts-Khulais, King Abdulaziz University, Jeddah, Saudi Arabia

[c] Department of Mathematics, Faculty of Science, Sahag University, Sohag, Egypt

[1] rajneesh_kuk@rediffmail.com

[2] ibrabbas7@yahoo.com

УДК 539.4

Возмущения от термомеханических источников в пористой термоупругой среде

Р. Кумар[а], И. А. Аббас[б,в]

[а] Отделение математики университета Курукшетра, Харьяна, Индия

[б] Отделение математики университета Кинг Абдулазиз, Джедда, Саудовская Аравия

[в] Отделение математики университета г. Сохаг, Египет

Исследована двухмерная задача о возникновении возмущений от механических и термических источников в однородной теплопроводящей пористо-упругой среде. Для решения этой задачи использованы преобразования Лапласа и Фурье. Для демонстрации перспективности данного подхода рассмотрены различные случаи с точечными и распределенными источниками. С помощью методики численной инверсии выполнены преобразования компонент перемещений, напряжений, давления в порах и температурных флуктуаций. Влияние пористости на указанные параметры представлено в виде графиков. Рассмотрены некоторые специальные случаи, имеющие практический интерес.

Ключевые слова: пористая термоупругая среда, преобразование Лапласа, преобразование Фурье, точечный источник, равномерно распределенный источник, линейно распределенный источник.

Introduction. Coupled thermal and poro-mechanical processes play an important role in a number of problems of interest in the geomechanics such as stability of borehole and permeability enhancement in geothermal reservoirs or high temperature petroleum bearing formations. A thermoporoelastic approach combine the theory of heat conduction with poroelastic constitutive equations and coupling the temperature field with the stresses and pore pressure.

Most of the modern engineering structures are generally made up of multiphase porous continuum, the classical theory, which represent a fluid saturated porous medium as a single phase material, is inadequate to represent the mechanical behavior of such material especially when the pore are filled with liquid. In this context the solid and liquid phases have different motions. Due to these different motions, the different material properties and the complicated geometry of pore structures, the mechanical behavior of a fluid saturated porous medium is very complex and difficult.

Based on the work of von Terzaghi [1, 2], Biot [3] proposed a general theory of three-dimensional deformations of liquid saturated porous solid. The Biot theory is based on the assumption of compressible constituents and till recently, some of his results have taken as standard references and basis for subsequent analysis in acoustic, geophysics, and other such fields [4–6].

Kumar and Hundal [7] discussed the wave propagation in a fluid saturated incompressible porous medium. Bai and Li [8] found a solution for cylindrical cavity in saturated thermoporoelastic medium by using Laplace transform and numerical Laplace transform inversion. Bai [9–11] discussed different thermal source problem in a saturated porous media.

Kaushal et al. [12] studied the response of frequency domain in generalized thermoelasticity with two temperature. Jabbari and Dehbani [13, 14] studied axisymmetric and spherical symmetric problems in porothermoelastic solids. Abbas [15] studied the natural frequencies of a poroelastic hollow cylinder. The counterparts of our problem in the contexts of the thermoelasticity theories have been considered by using analytical and numerical methods [16–29].

In the present paper, we obtain the components of displacement, stress, pore pressure and temperature change due to concentrated source and distributed source in thermoporoelastic medium. Laplace and Fourier transforms are used to investigate the problem. Numerical inversion technique is applied to obtain the resulting quantities in a physical domain. The resulting quantities are shown graphically to depict the effect of porosity.

Governing Equations. Following Jabbari and Dehbani [30], the field equations are

$$(\lambda+\mu)\nabla\nabla\vec{u}+\mu\nabla^2\vec{u}-\alpha\nabla p-\beta\nabla T=\rho\frac{\partial^2\vec{u}}{\partial t^2}, \tag{1}$$

$$\frac{k}{\gamma_w}\nabla^2 p-\alpha_p\dot{p}-Y\dot{T}-\alpha\,\mathrm{div}\,\dot{\vec{u}}=0, \tag{2}$$

$$K\nabla^2 T-ZT_0\dot{T}+YT_0\dot{p}-\beta T_0\,\mathrm{div}\,\dot{\vec{u}}=0, \tag{3}$$

$$\sigma_{ij}=\lambda u_{k,k}\delta_{ij}+\mu(u_{i,j}+u_{j,i})-\alpha p\delta_{ij}-\beta T\delta_{ij}, \tag{4}$$

where $\vec{u}$ is the displacement component, p is the pore pressure, ρ is the bulk mass density, $\alpha=1-C_s/C$ is the Biot coefficient, $C_s=3(1-2\nu_s)/E_s$ is the coefficient of volumetric compression of solid grain, with E_s and ν_s being the elastic modulus and Poisson's ratio of solid grain, $C=3(1-2\nu)/E$ is the coefficient of volumetric compression of solid skeleton, with E and ν being the elastic modulus and Poisson's ratio of solid skeleton, T_0 is initial reference temperature, $\beta=3\alpha_s/C$ is the thermal expansion factor, α_s is the coefficient of linear thermal expansion of solid grain, $Y=3(n\alpha_w+(\alpha-n)\alpha_s)$ and $\alpha_p=n(C_w-C_s)+\alpha C_s$ are coupling parameters, α_w and C_w are the coefficients of linear thermal expansion and volumetric compression of pure water, n is the porosity, k is the hydraulic conductivity, γ_w is the unit of pore water, $Z=\dfrac{(1-n)\rho_s c_s+n\rho_w c_w}{T_0}-3\beta\alpha_s$ is coupling parameter, ρ_w and ρ_s are densities of pore water and solid grain, c_w and c_s are heat capacities of pore water and solid grain, and K is the coefficient of heat conductivity.

Formulation of the Problem. We consider homogeneous porothermoelastic half space $x_3\geq 0$ of a rectangular Cartesian coordinate system (x_1, x_2, x_3) having origin at the surface $x_3=0$, x_3 is the axis pointing vertically downward in the medium. A mechanical

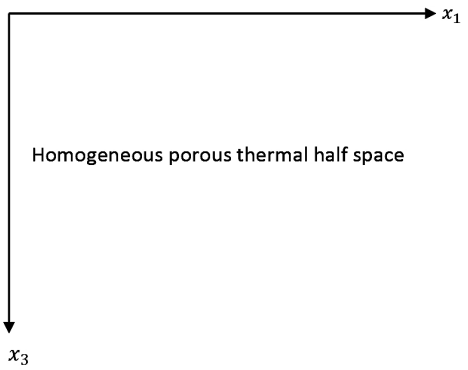

Fig. 1. Geometry of the problem.

or thermal source is assumed to be acting at the origin. We restrict our analysis to the plane strain parallel to $x_1 - x_3$ plane. The complete geometry of the problem is shown in Fig. 1.

For two-dimensional problem we take the displacement vector $\vec{u}$ as

$$\vec{u} = (u(x_1, x_3), 0, w(x_1, x_3)). \tag{5}$$

To facilitate the solution, the following dimensionless quantities are introduced as

$$\begin{gathered} x_1' = \frac{\omega^*}{c_1} x_1, \quad x_3' = \frac{\omega^*}{c_1} x_3, \quad u_1' = \frac{\omega^* \rho c_1}{\beta T_0} u_1, \quad u_3' = \frac{\omega^* \rho c_1}{\beta T_0} u_3, \quad p' = \frac{p}{\beta T_0}, \\ c_1^2 = \frac{\lambda + 2\mu}{\rho}, \quad t' = \omega^* t, \quad T' = \frac{T}{T_0}, \quad \omega^* = \frac{Z T_0 c_1^2}{K}, \quad \sigma_{33}' = \frac{\sigma_{33}}{\beta T_0}, \quad \sigma_{31}' = \frac{\sigma_{31}}{\beta T_0}. \end{gathered} \tag{6}$$

The expressions relating the displacement components $u_1(x_1, x_3, t)$ and $u_3(x_1, x_3, t)$ to the scalar potentials Φ and Ψ in dimensionless form are given by

$$u_1 = \frac{\partial \Phi}{\partial x_1} - \frac{\partial \Psi}{\partial x_3}, \qquad u_3 = \frac{\partial \Phi}{\partial x_3} + \frac{\partial \Psi}{\partial x_1}. \tag{7}$$

We define the Laplace and Fourier transforms as follows:

$$\bar{f}(s) = \int_0^\infty f(t) e^{-st} dt, \tag{8}$$

$$\tilde{\bar{f}}(\xi) = \int_{-\infty}^{\infty} \bar{f}(\xi) e^{i\xi x_1} dx. \tag{9}$$

Applying Laplace and Fourier transforms defined by (8) and (9) on Eqs. (1)–(3) and with the aid of (5)–(7) and after some simplifications we obtain

$$\left[A_1 \frac{d^6}{dx_3^6} + A_2 \frac{d^4}{dx_3^4} + A_3 \frac{d^2}{dx_3^2} + A_4 \right] \tilde{\bar{\Phi}} = 0, \tag{10}$$

$$a_1 \left(\frac{d^2}{dx_3^2} - \xi^2 \right) \tilde{\bar{\Psi}} - a_4 s^2 \tilde{\bar{\Psi}} = 0, \tag{11}$$

where

$$A_1 = b_1 b_4 (1+a_1),$$

$$A_2 = 3\xi^2 b_1 b_4 (1+a_1) - s(1+a_1)(b_1 b_5 + b_2 b_4) - a_4 b_1 b_4 s^2 - a_2 b_4 s - a_3 b_1 s,$$

$$A_3 = 3\xi^4 b_1 b_4 (1+a_1) + 2\xi^2 s(1+a_1)(b_1 b_5 + b_2 b_4) + s^2(1+a_1)(b_1 b_5 + b_2 b_4) +$$

$$+ 2\xi^2 s^2 a_4 b_1 b_4 + a_4 s^3 (b_1 b_5 + b_2 b_4) + 2\xi^2 a_2 b_4 s - a_2 s^2 (b_3 - b_5) +$$

$$+ 2\xi^2 a_3 b_1 s + a_3 s^2 (b_6 + b_2),$$

$$A_4 = -\xi^6 b_1 b_4 (1+a_1) - s\xi^4 (1+a_1)(b_1 b_5 + b_2 b_4) + s^2 \xi^2 (1+a_1)(b_1 b_5 + b_2 b_4) -$$

$$- a_4 b_1 b_4 s^2 \xi^4 - a_4 s^3 \xi^2 (b_1 b_5 + b_2 b_4) - a_4 s^4 (b_2 b_5 + b_3 b_6) - a_2 b_4 s\xi^4 +$$

$$+ a_2 s^2 (b_3 - b_5)\xi^2 - \xi^4 a_3 b_1 s - a_3 s^2 \xi^2 (b_6 + b_2),$$

$$a_1 = \frac{\mu}{\lambda+\mu}, \quad a_2 = \frac{\alpha\rho c_1^2}{\lambda+\mu}, \quad a_3 = \frac{\rho c_1^2}{(\lambda+\mu)}, \quad a_4 = \frac{\rho c_1^2}{\lambda+\mu},$$

$$b_1 = \frac{k\omega^* \beta T_0}{\gamma_w \alpha c_1^2}, \quad b_2 = \frac{\alpha_p \beta T_0}{\alpha}, \quad b_3 = \frac{YT_0}{\alpha}, \quad b_4 = \frac{K\omega^*}{\beta c_1^2}, \quad b_5 = \frac{ZT_0}{\beta}, \quad b_6 = YT_0.$$

The solution of Eqs. (10) and (11) satisfying the radiation conditions that $\widetilde{\widetilde{\Phi}}, \widetilde{\widetilde{\Psi}}, \widetilde{\widetilde{p}}$, and $\widetilde{\widetilde{T}} \to 0$ as $x_3 \to \infty$ we obtain the value of $\widetilde{\widetilde{\Phi}}, \widetilde{\widetilde{\Psi}}, \widetilde{\widetilde{p}}$, and $\widetilde{\widetilde{T}}$ as

$$(\widetilde{\widetilde{\Phi}}, \widetilde{\widetilde{p}}, \widetilde{\widetilde{T}}) = \Sigma_{i=1}^{3} (1, r_i, s_i) B_i e^{-m_i x_3}, \tag{12}$$

$$\widetilde{\widetilde{\Psi}} = B_4 e^{-m_4 x_3}, \tag{13}$$

where m_1, m_2, and m_3 are the roots of Eq. (10), and $m_4 = \sqrt{A_5}$, $A_5 = \xi^2 + \frac{a_4}{a_1} s^2$, and the coupling constants are given by

$$r_i = \frac{b_4 s(m_i^2 - \xi^2)^2 + (b_3 s^2 - b_5 s^2)(m_i^2 - \xi^2)}{b_1 b_4 (m_i^2 - \xi^2)^2 - (b_1 b_5 s + b_2 b_4 s)(m_i^2 - \xi^2) + (b_2 b_5 s^2 + b_3 b_6 s^2)}, \tag{14}$$

$$s_i = \frac{b_1 s(m_i^2 - \xi^2)^2 - (b_6 s^2 + b_2 s^2)(m_i^2 - \xi^2)}{b_1 b_4 (m_i^2 - \xi^2)^2 - (b_1 b_5 s + b_2 b_4 s)(m_i^2 - \xi^2) + (b_2 b_5 s^2 + b_3 b_6 s^2)} \quad (i = 1, 2, 3). \tag{15}$$

The displacement components $\widetilde{\widetilde{u}}_1$ and $\widetilde{\widetilde{u}}_3$ are obtained with the aid of (7)–(9) and (12), (13) as

$$\widetilde{\widetilde{u}}_1 = -B_1 i\xi e^{-m_1 x_3} - B_2 i\xi e^{-m_2 x_3} - B_3 i\xi e^{-m_3 x_3} + B_4 m_4 e^{-m_4 x_3}, \tag{16}$$

$$\tilde{\tilde{u}}_3 = -B_1 m_1 e^{-m_1 x_3} - B_2 m_2 e^{-m_2 x_3} - B_3 m_3 e^{-m_3 x_3} - B_4 i\xi e^{-m_4 x_3}. \tag{17}$$

Boundary Conditions and Solution of the Problem. The boundary conditions at $x_3 = 0$ are

$$\begin{gathered} \sigma_{33} = -F_1 F(x_1) H(t), \qquad \sigma_{31} = -F_2 F(x_1) H(t), \\ p = F_3 F(x_1) H(t), \qquad \frac{\partial T}{\partial x_3} = F_4 F(x_1) H(t), \end{gathered} \tag{18}$$

where F_1 and F_2 are the magnitudes of the vertical and horizontal forces, respectively, F_3 is the constant pressure applied on the boundary, F_4 is the constant temperature applied on the boundary, $F(x_1)$ is a known function, and $H(t)$ is the Heaviside unit step function.

Applying Laplace and Fourier transforms defined by (8) and (9) on (18) and with the aid of (4), (5), and (10), and

$$F_i' = \frac{F_i}{\beta T_0} \qquad (i = 1, 2, 3) \qquad \text{and} \qquad F_4' = \frac{F_4 c_1}{\omega^* T_0},$$

we obtain

$$\begin{gathered} \tilde{\tilde{\sigma}}_{33} = -F_1 \tilde{\tilde{F}}(\xi)/s, \qquad \tilde{\tilde{\sigma}}_{31} = -F_2 \tilde{\tilde{F}}(\xi)/s, \qquad \tilde{\tilde{p}} = F_3 \tilde{\tilde{F}}(\xi)/s, \\ \frac{\partial T}{\partial x_3} = F_4 \tilde{\tilde{F}}(\xi)/s \qquad \text{at} \qquad x_3 = 0, \end{gathered} \tag{19}$$

where

$$\tilde{\tilde{\sigma}}_{33} = -R_1 i\xi \tilde{\tilde{u}}_1 + R_2 \frac{d\tilde{\tilde{u}}_3}{dx_3} - \alpha \tilde{\tilde{p}} - \beta \tilde{\tilde{T}}, \tag{20}$$

$$\tilde{\tilde{\sigma}}_{31} = R_3 \left[\frac{d\tilde{\tilde{u}}_1}{dx_3} - i\xi \tilde{\tilde{u}}_3 \right], \tag{21}$$

and

$$R_1 = \frac{\lambda}{\rho c_1^2}, \; R_2 = \frac{\lambda + 2\mu}{\rho c_1^2}, \; R_3 = \frac{\mu}{\rho c_1^2}.$$

Case 1: For normal force $F_2 = F_3 = F_4 = 0$.
Case 2: For tangential force $F_1 = F_3 = F_4 = 0$.
Case 3: For pressure source $F_1 = F_2 = F_4 = 0$.
Case 4: For thermal source $F_1 = F_2 = F_3 = 0$.

Substituting the values of $\tilde{\tilde{u}}_1$, $\tilde{\tilde{u}}_3$, $\tilde{\tilde{p}}$, and $\tilde{\tilde{T}}$ from (16), (17), and (12) in the boundary condition (19) and with help of (20) and (21), after some simplifications, we obtain

$$\tilde{\tilde{\sigma}}_{33} = \frac{1}{s\Delta} \tilde{\tilde{F}}(\xi) [d_1 \Delta_1 e^{-m_1 x_3} + d_2 \Delta_2 e^{-m_2 x_3} + d_3 \Delta_3 e^{-m_3 x_3} + d_4 \Delta_4 e^{-m_4 x_3}], \tag{22}$$

$$\tilde{\tilde{\sigma}}_{31} = \frac{1}{s\Delta} \tilde{\tilde{F}}(\xi) [d_5 \Delta_1 e^{-m_1 x_3} + d_6 \Delta_2 e^{-m_2 x_3} + d_7 \Delta_3 e^{-m_3 x_3} + d_8 \Delta_4 e^{-m_4 x_3}], \tag{23}$$

$$\tilde{\tilde{p}} = \frac{1}{s\Delta}\tilde{\tilde{F}}(\xi)[r_1\Delta_1 e^{-m_1 x_3} + r_2\Delta_2 e^{-m_2 x_3} + r_3\Delta_3 e^{-m_3 x_3}], \tag{24}$$

$$\tilde{\tilde{T}} = \frac{1}{s\Delta}\tilde{\tilde{F}}(\xi)[s_1\Delta_1 e^{-m_1 x_3} + s_2\Delta_2 e^{-m_2 x_3} + s_3\Delta_3 e^{-m_3 x_3}], \tag{25}$$

where

$$\Delta = d_1 d_8(-m_3 r_2 s_3 + m_2 r_3 s_2) - d_2 d_8(-m_3 r_1 s_3 + m_1 r_3 s_1) + d_3 d_8(-m_2 r_1 s_2 + m_1 r_2 s_1) -$$

$$- d_4 d_5(-m_3 r_2 s_3 + m_2 r_3 s_2) - d_4 d_6(-m_1 r_3 s_1 + m_3 r_1 s_3) - d_4 d_7(-m_2 r_1 s_2 + m_1 r_2 s_1),$$

$$d_i = -R_1\xi^2 + R_2 m_i^2 - \alpha r_i - s_i \qquad (i = 1, 2, 3), \qquad d_4 = i\xi m_4(-R_1 + R_2),$$

$$d_j = 2i\xi m_j R_3 \qquad (j = 5, 6, 7), \qquad d_8 = -R_3(m_4^2 + \xi^2),$$

and Δ_1, Δ_2, Δ_3, and Δ_4 are obtained by replacing $[-F_1, -F_2, F_3, F_4]^T$ in Δ.

Applications.

Case 1. ***Concentrated Source***. The values for displacement, stress, pore pressure and temperature change presented in Eqs. (22)–(25) will used to yield the response over the half space subjected to a concentrated source as

$$F(x_1) = \delta(x_1), \tag{26}$$

where $\delta(\cdot)$ is the Dirac delta function.

Applying the Laplace and Fourier transforms defined by (8) and (9) on (26), yield

$$\tilde{\tilde{F}}(\xi) = 1. \tag{27}$$

The component of displacement, stress, pore pressure, and temperature change are obtained by using (27) in (22)–(25).

Case 2. ***Influence Function***. Here

$$F(x_1) = \Psi_1(x_1), \tag{28}$$

where $\Psi_1(x_1)$ is a known function, which can have two types of values:

1. Uniformly distributed source,

$$\Psi_1(x_1) = \begin{Bmatrix} 1, & |x_1| \le a \\ 0, & |x_1| > a \end{Bmatrix}, \tag{29}$$

where $2a$ is non-dimensional width of the strip.

Applying the Laplace and Fourier transforms defined by (8) and (9) on (28) and (29), we obtain

$$\tilde{\tilde{F}}(\xi) = (2\sin\xi a)/\xi. \tag{30}$$

2. Linearly distributed source,

$$\Psi_1(x_1) = \begin{Bmatrix} 1 - |x_1|/a, & |x_1| \le a \\ 0, & |x_1| > a \end{Bmatrix}. \tag{31}$$

Applying the Laplace and Fourier transforms defined by (8) and (9) on (28) and (31), we obtain

$$\overline{\overline{F}}(\xi, s) = \frac{2[1-\cos(\xi a)]}{\xi^2 a}. \tag{32}$$

The expression for stresses, pore pressure and temperature field are obtained for concentrated, uniformly and linearly distributed sources by replacing $\overline{\overline{F}}(\xi)$ from (27), (30), and (32) in (22)–(25).

Special Case. In the absence of porosity effect, the boundary conditions reduce to

$$\overline{\overline{\sigma}}_{33} = -F_1\overline{\overline{F}}(\xi)/s, \qquad \overline{\overline{\sigma}}_{31} = -F_2\overline{\overline{F}}(\xi)/s, \qquad \frac{\partial T}{\partial x_3} = F_4\overline{\overline{F}}(\xi)/s, \tag{33}$$

and we obtain the corresponding expressions for stress components and temperature field in thermoelastic half space are obtained as

$$\overline{\overline{\sigma}}_{zz} = \frac{1}{s\Delta_{10}}\overline{\overline{F}}(\xi)[d_9\Delta_5 e^{-m_5x_3} + d_{10}\Delta_6 e^{-m_6x_3} + d_4\Delta_7 e^{-m_4x_3}], \tag{34}$$

$$\overline{\overline{\sigma}}_{zr} = \frac{1}{s\Delta_{10}}\overline{\overline{F}}(\xi)[d_{11}\Delta_5 e^{-m_5x_3} + d_{12}\Delta_6 e^{-m_6x_3} + d_8\Delta_7 e^{-m_4x_3}], \tag{35}$$

$$\overline{\overline{T}} = \frac{1}{s\Delta_{10}}\overline{\overline{F}}(\xi)[r_5\Delta_5 e^{-m_5x_3} + r_6\Delta_6 e^{-m_6x_3}], \tag{36}$$

where

$$d_9 = -R_1\xi^2 + R_2m_5^2 - r_5, \qquad d_{10} = -R_1\xi^2 + R_2m_6^2 - r_6, \qquad d_{11} = 2i\xi m_5R_3,$$

$$d_{12} = 2i\xi m_6R_3, \qquad \Delta_{10} = d_9d_8m_6r_6 - d_{10}d_8m_5r_5 - d_4d_{11}m_6r_6 + d_4d_{12}m_5r_5,$$

and Δ_5, Δ_6, and Δ_7 are obtained by replacing $[-F_1, -F_2, F_4]^T$ in Δ_{10}.

Taking $F_2 = F_4 = 0$, $F_1 = F_4 = 0$, and $F_1 = F_2 = 0$ in Eqs. (34), (35), and (36), respectively, we obtain the stress components and temperature change for normal force, tangential forces, and thermal source, respectively.

Inversion of the Transform. The transformed displacements, stresses, pore pressure and temperature field are functions of the parameters of the Laplace and Fourier transforms s and ξ, respectively, and hence are of the form $\overline{\overline{f}}(\xi, x_3, s)$. To obtain the solution of the problem in the physical domain, we invert the Laplace and Fourier transforms by using the method described by Kumar and Rani [31].

Numerical Results and Discussion. Following Jabbari and Dehbani [30], for numerical computation, we take the value of the various physical parameters as $E = 6\cdot10^5$ MPa, $\nu = 0.3$, $T_0 = 293$ K, $K_s = 2\cdot10^{10}$, $K_w = 5\cdot10^9$, $K = 0.5$, $\alpha_s = 1.5\cdot10^{-5}$, $\alpha_W = 2\cdot10^{-4}$, $c_s = 0.8$, $c_w = 4.2$, $\rho_s = 2.6\cdot10^6$, $\rho_w = 1\cdot10^6$, $\alpha = 1$, $F_1 = F_2 = F_3 = F_4 = 1$.

The values of normal stress σ_{33}, tangential stress σ_{31}, pore pressure p, and temperature change T for incompressible fluid saturated thermoporoelastic medium (FSPM) and empty porous thermoelastic medium (EPM) are shown due to concentrated source (CS), uniformly distributed source (UDS), and linearly distributed source (LDS). The

computation are carried out for two values of dimensionless time $t = 0.01$ and 0.05 at $x_3 = 1$ for the range $0 \le x_1 \le 10$, and $a = 1$.

The solid lines either with or with central symbols represents the variations for $t = 0.01$, whereas the dashed lines with or without central symbols represents the variations for $t = 0.05$. Curves without central symbols correspond to the case of FSPM whereas those with central symbols corresponds to the case of EPM.

Figure 2a shows the variation of normal stress component σ_{33} w.r.t distance x_1 for both FSPM and EPM due to concentrated normal force. The value of σ_{33} start with initial decrease and remain close to the boundary surface for FSPM as x_1 increases and in case of EPM, its value decrease in the range $0 \le x \le 3$ and then oscillates as x_1 increases for both values of time.

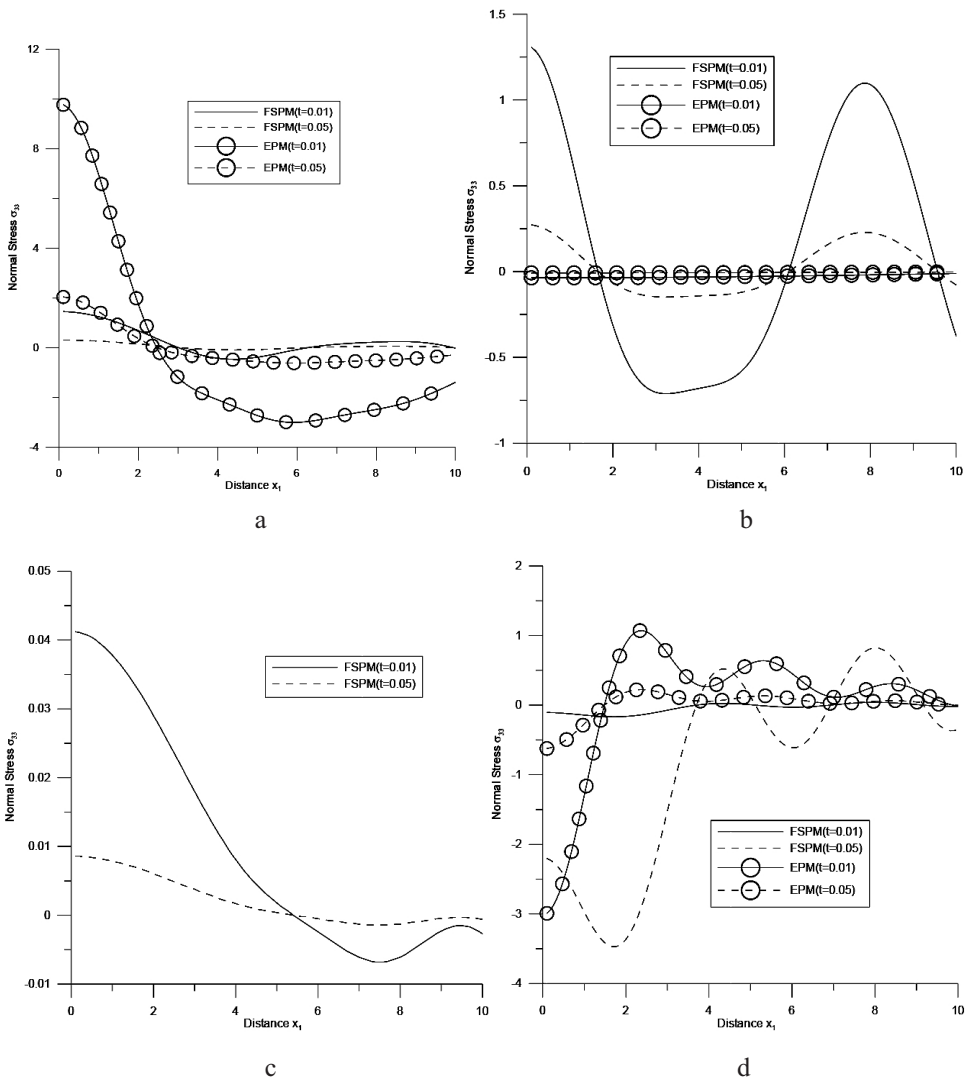

Fig. 2. Variation of normal stress σ_{33} with distance x_1 due to concentrated normal force (a), concentrated tangential force (b), concentrated pressure source (c), and thermal source (d).

Figure 2b shows the variation of normal stress component σ_{33} w.r.t distance x_1 for both FSPM and EPM due to concentrated tangential force. The value of σ_{33} first decrease

in the range $0 \le x_1 \le 4$ and then starts oscillating for FSPM as x_1 increases for both values of time whereas in case of EPM, the value of σ_{33} remain close to the boundary surface for different values of time as x_1 increases.

Figure 2c shows the variation of normal stress component σ_{33} w.r.t distance x_1 for FSPM due to concentrated pressure source. The value of σ_{33} decrease in the range $0 \le x_1 \le 7.5$ and then starts increasing for different values of time.

Figure 2d shows the variation of normal stress component σ_{33} w.r.t distance x_1 for FSPM and EPM due to thermal source. The value of σ_{33} oscillates for different value of time for FSPM as x_1 increases whereas in case of EPM, the value of σ_{33} first increases in the range $0 \le x_1 \le 2.2$ and then starts oscillating for both values of time.

Figure 3a shows the variation of pore pressure p w.r.t distance x_1 for FSPM due to concentrated normal force. Near the application of the source the value of p is more for the time $t = 0.05$ as compared to time $t = 0.01$ and away from the source reverse behavior is noticed.

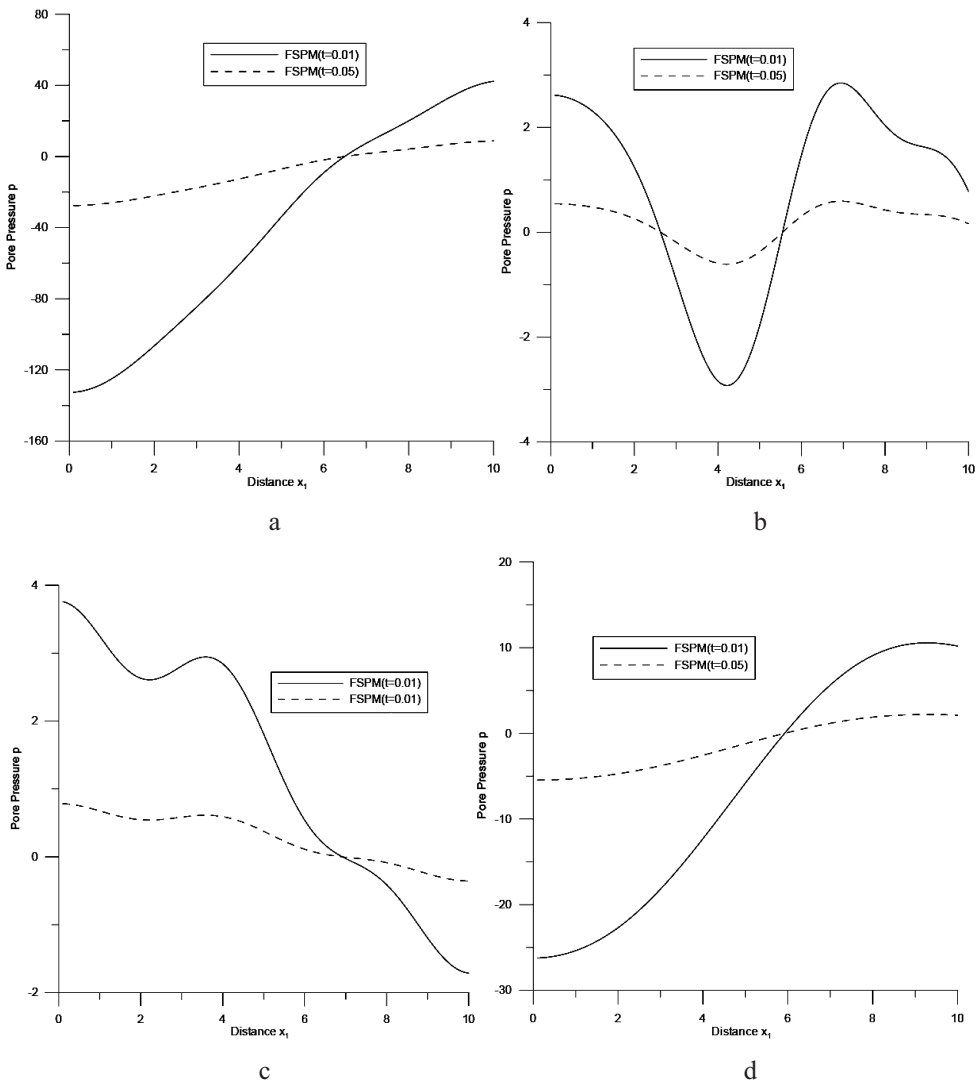

Fig. 3. Variation of pore pressure p with distance x_1 due to concentrated normal force (a), concentrated tangential force (b), concentrated pressure source (c), and thermal source (d).

Figure 3b shows the variation of pore pressure p w.r.t distance x_1 for FSPM due to concentrated tangential force. The value of p first decreases in the range $0 \le x_1 \le 4.2$ and then starts increasing for different values of time.

Figure 3c shows the variation of pore pressure p w.r.t distance x_1 for FSPM due to concentrated pressure source. The value of p starts decreasing as x_1 increases for different values of time.

Figure 3d shows the variation of pore pressure p w.r.t distance x_1 for FSPM due to thermal source. For the time $t = 0.05$ the value of p is higher in the range $0 \le x_1 \le 6$ whereas for the time $t = 0.01$ the value of p is higher in the range $6 \le x_1 \le 10$.

Figure 4a shows the variation of temperature T w.r.t distance x_1 for FSPM and EPM due to concentrated normal force. The value of T first decreases and then oscillates for FSPM as x_1 increases for both value of time whereas for EPM it first increases in the range $0 \le x_1 \le 3.5$ and then oscillates for both values of time.

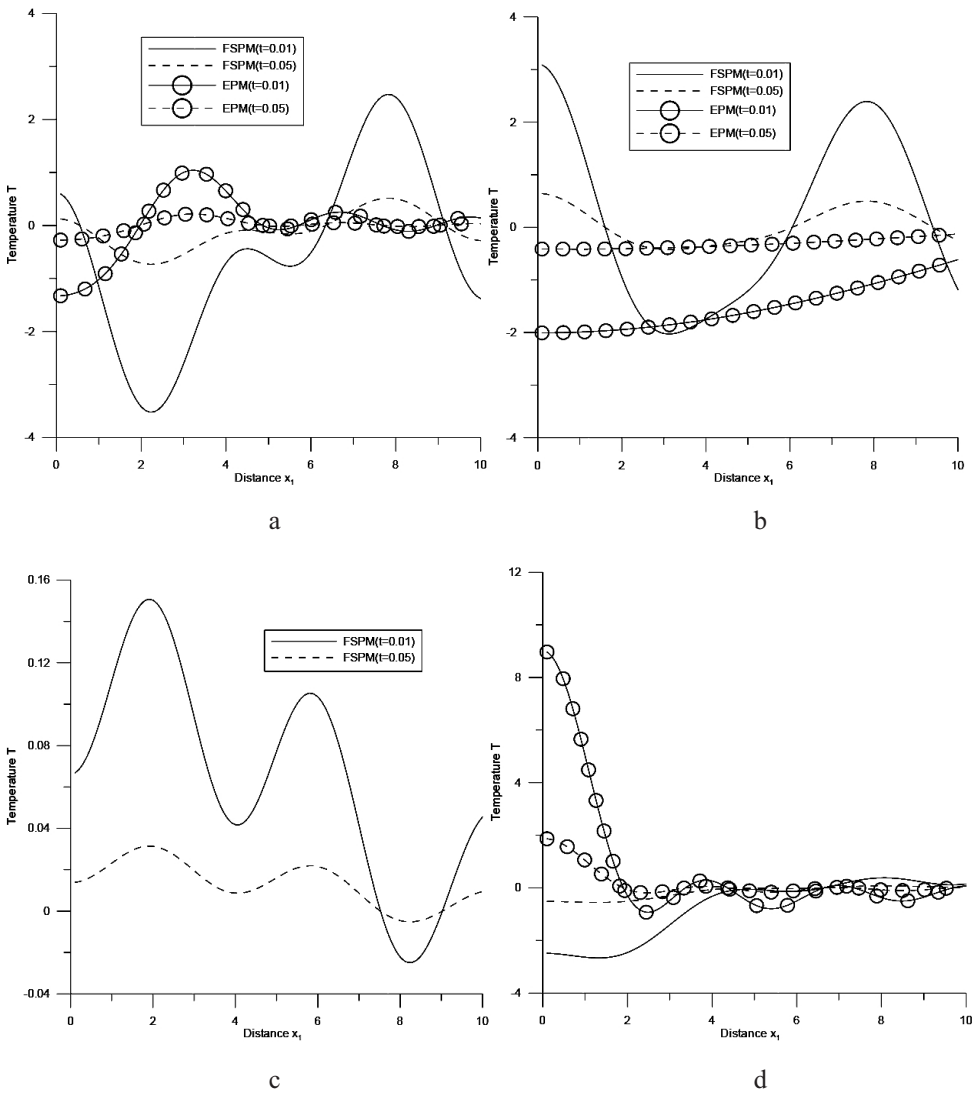

Fig. 4. Variation of temperature T with distance x_1 due to concentrated normal force (a), concentrated tangential force (b), concentrated pressure source (c), and thermal source (d).

Figure 4b shows the variation of temperature T w.r.t distance x_1 for FSPM and EPM due to tangential force. The value of T first decreases and then oscillates for FSPM and for EPM shows a small increase as x_1 increases for different values of time.

Figure 4c shows the variation of temperature T w.r.t distance x_1 for FSPM due to pressure source. The value of T starts oscillates for the time $t = 0.01$ and 0.05.

Figure 4d shows the variation of temperature T w.r.t distance x_1 for FSPM and EPM due to thermal source. The value of T first increases and remains close to zero for FSPM as x_1 increases for both value time whereas for EPM the value of T decreases in the range $0 \le x_1 \le 2.5$ and then starts oscillates for both value of time as x_1 increases.

Figure 5a shows the variation of normal stress component σ_{33} w.r.t distance x_1 for FSPM and EPM due to normal force over uniformly distributed source. The value of σ_{33} for FSPM first decreases in the range $0 \le x_1 \le 4.5$ and then oscillates for both value of time whereas for EPM its value shows a small decrease for both values of time as x_1 increases.

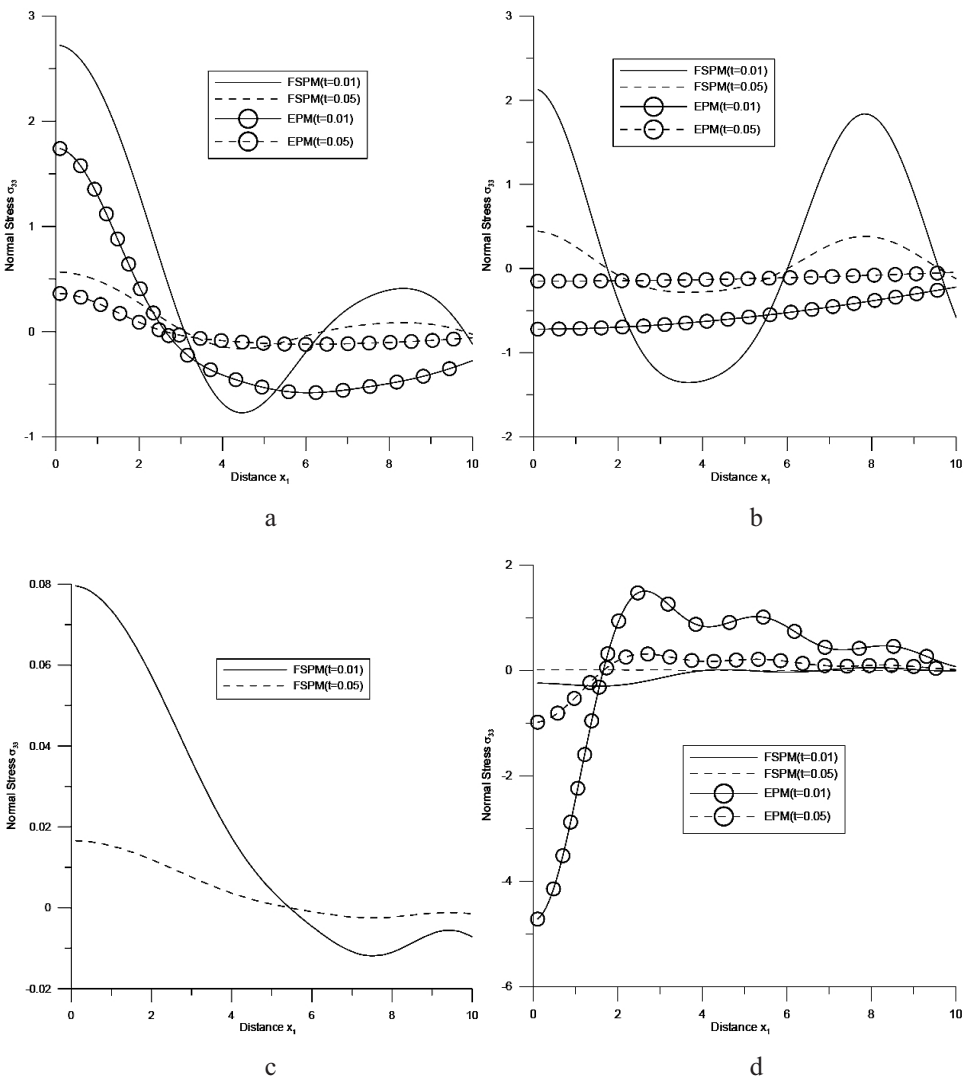

Fig. 5. Variation of normal stress σ_{33} with distance x_1 due to concentrated normal force (a), concentrated tangential force (b), concentrated pressure source (c), and thermal source (d).

Figure 5b shows the variation of normal stress component σ_{33} w.r.t distance x_1 for FSPM and EPM due to tangential force over uniformly distributed source. The value of σ_{33} first decreases in the range $0 \le x_1 \le 4$ and then oscillates for FSPM as x_1 increases for both value of time where as for EPM its value shows a small increase as x_1 increases for different values of time.

Figure 5c shows the variation of normal stress component σ_{33} w.r.t distance x_1 for FSPM due to pressure source over uniformly distributed source. The value of σ_{33} shows a sharp decrease in the range $0 \le x_1 \le 7.6$ for FSPM as x_1 increases for both values of time.

Figure 5d shows the variation of normal stress component σ_{33} w.r.t distance x_1 for FSPM and EPM due to thermal source over uniformly distributed source. The value of σ_{33} remain close to zero for FSPM as x_1 increases for both value of time whereas the value of σ_{33} first increases in the range $0 \le x_1 \le 2.2$ and then oscillates for EPM as x_1 increases for the time $t = 0.01$ and 0.05.

Figure 6a shows the variation of pore pressure p w.r.t distance x_1 for FSPM due to normal force over uniformly distributed source. The value of p shows a sharp increase for FSPM for different values of time as x_1 increases.

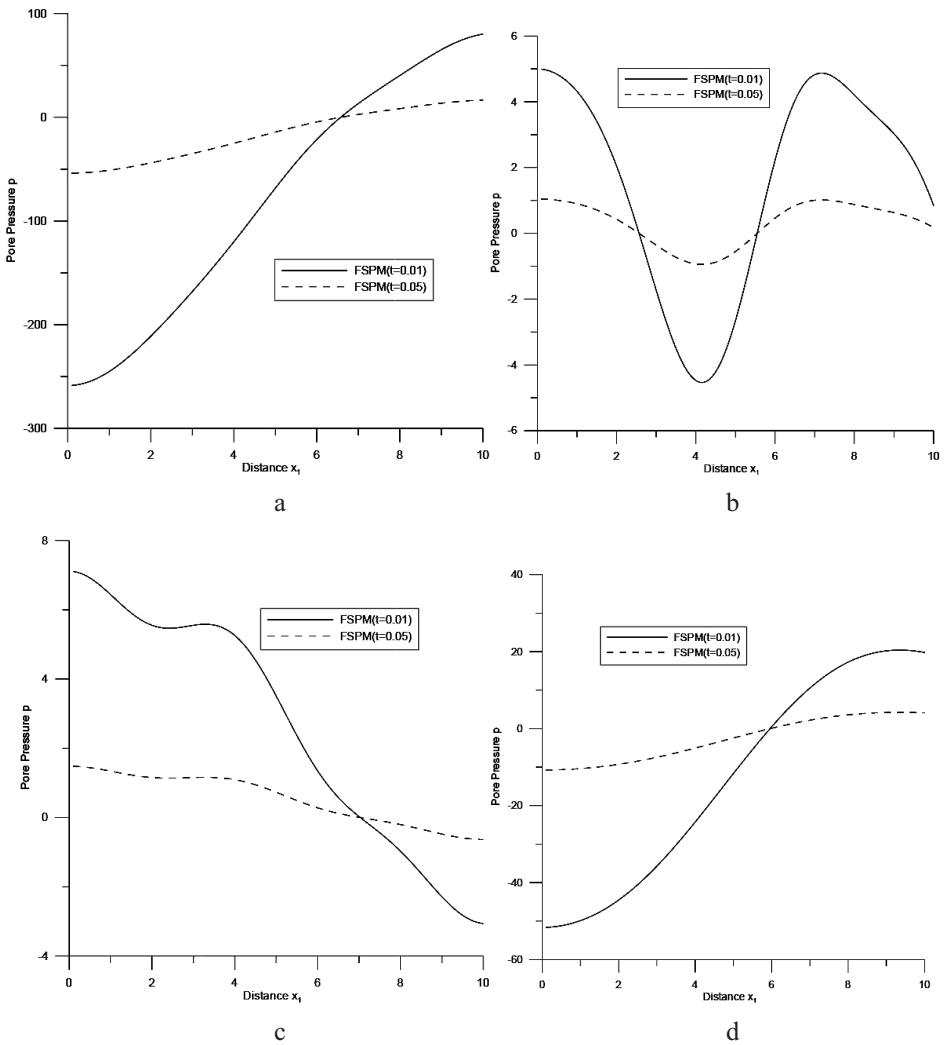

Fig. 6. Variation of pore pressure p with distance x_1 due to concentrated normal force (a), concentrated tangential force (b), concentrated pressure source (c), and thermal source (d).

Figure 6b shows the variation of pore pressure p w.r.t distance x_1 for FSPM due to tangential force over uniformly distributed source. The value of p first decreases in the range $0 \le x_1 \le 4.2$ and then increases as x_1 increases for FSPM for the time $t = 0.01$ and 0.05.

Figure 6c shows the variation of pore pressure p w.r.t distance x_1 for FSPM due to pressure source over uniformly distributed source. The value of p shows a sharp decrease for FSPM as x_1 increases for different values of time.

Figure 6d shows the variation of pore pressure p w.r.t distance x_1 for FSPM due to thermal source over uniformly distributed source. For the time $t = 0.05$ the value of p is more in the range $0 \le x_1 \le 6$ whereas for the time $t = 0.01$ the value of p is more in the range $6 \le x_1 \le 10$.

Figure 7a shows the variation of temperature T w.r.t distance x_1 for FSPM and EPM due to normal force over uniformly distributed source. The value of T first decreases and then oscillates for FSPM whereas for EPM the value of T first increases and then oscillates as x_1 increases for different values of time.

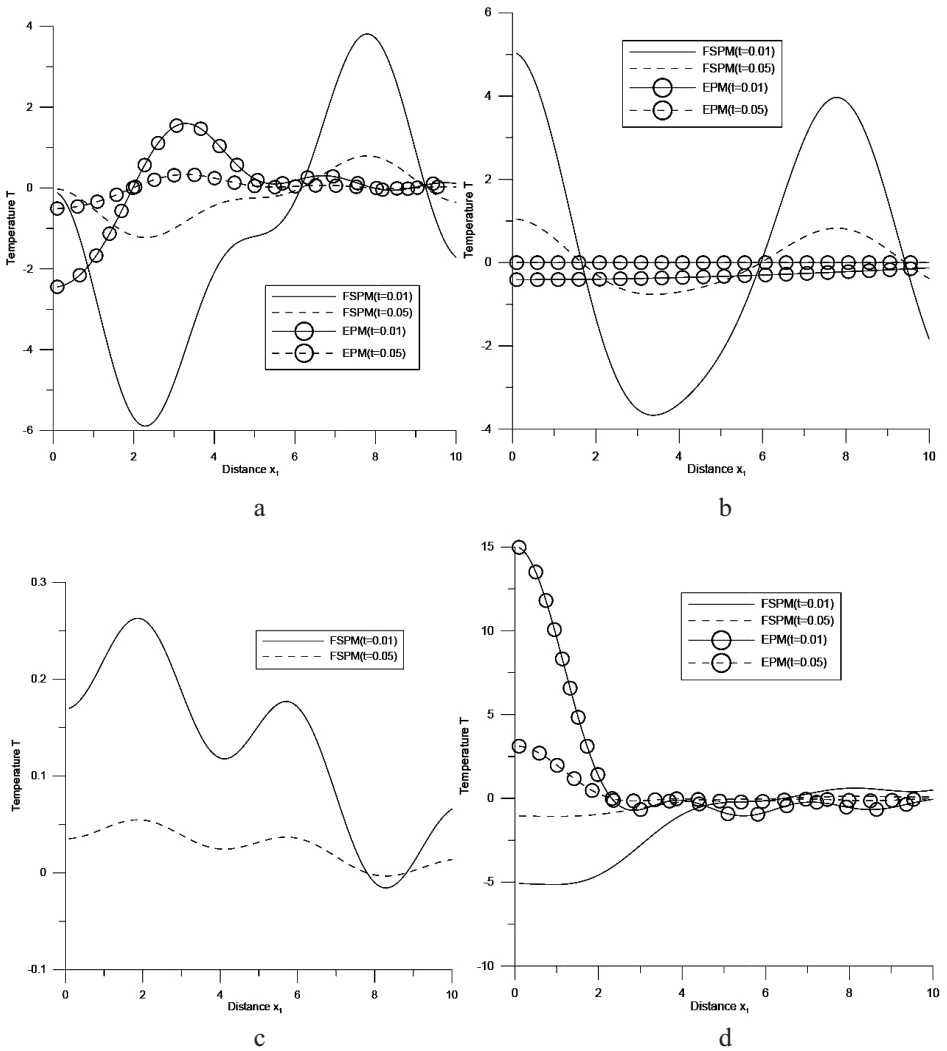

Fig. 7. Variation of temperature T with distance x_1 due to concentrated normal force (a), concentrated tangential force (b), concentrated pressure source (c), and thermal source (d).

Figure 7b shows the variation of temperature T w.r.t distance x_1 for FSPM and EPM due to tangential force over uniformly distributed source. The value of T first decreases and then start oscillates for FSPM and remain close to zero for EPM as x_1 increases for both values time.

Figure 7c shows the variation of temperature T w.r.t distance x_1 for FSPM due to pressure source over uniformly distributed source. The value of T first increases and then starts decreasing in oscillatory manner for FSPM as x_1 increases for the time $t = 0.01$ and 0.05.

Figure 7d shows the variation of temperature T w.r.t distance x_1 for FSPM and EPM due to thermal source over uniformly distributed source. The value of T first increases and remains close to zero for FSPM as x_1 increases for both value time whereas for EPM the value of T decreases in the range $0 \le x_1 \le 2.5$ and then oscillates for both value of time as x_1 increases.

Figure 8a shows the variation of normal stress component σ_{33} w.r.t distance x_1 for FSPM and EPM due to normal force over linearly distributed source. The value of σ_{33} remain close to zero for FSPM whereas for EPM it decreases in the range $0 \le x_1 \le 4$ and then becomes linear for both values of time as x_1 increases.

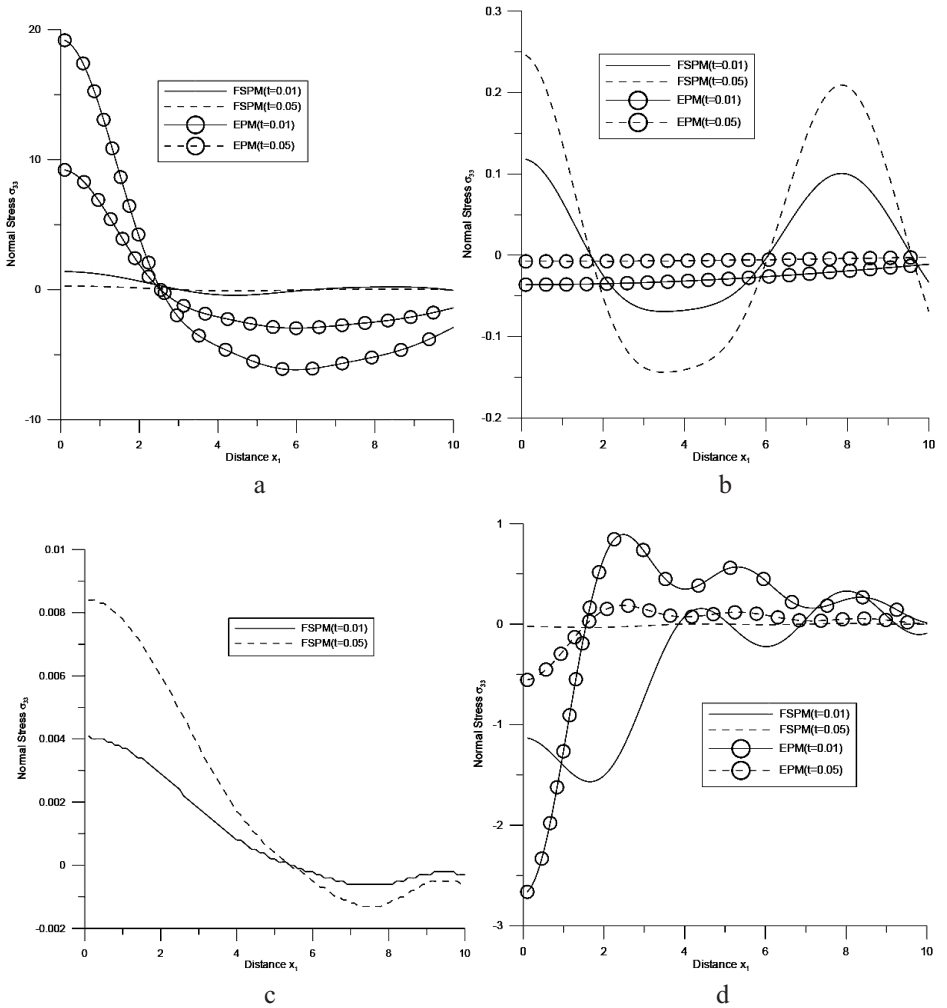

Fig. 8. Variation of normal stress σ_{33} with distance x_1 due to concentrated normal force (a), concentrated tangential force (b), concentrated pressure source (c), and thermal source (d).

Figure 8b shows the variation of normal stress component σ_{33} w.r.t distance x_1 for FSPM and EPM due to tangential force over linearly distributed source. The value of σ_{33} for FSPM first decreases in the range $0 \le x_1 \le 4$, increases in the range $4 \le x_1 \le 8$ whereas for EPM it remains close to zero for different values of time as x_1 increases.

Figure 8c shows the variation of normal stress component σ_{33} w.r.t distance x_1 for FSPM due to pressure source over linearly distributed source. The value of σ_{33} shows a sharp decrease in the range $0 \le x_1 \le 7.8$ and then increases for FSPM as x_1 increases for different values of time.

Figure 8d shows the variation of normal stress component σ_{33} w.r.t distance x_1 for FSPM and EPM due to thermal source over linearly distributed source. The value of σ_{33} oscillates for FSPM whereas the value of σ_{33} first increases in the range $0 \le x_1 \le 2$ and then oscillates for EPM as x_1 increases for both values of time.

Figure 9a shows the variation of pore pressure p w.r.t distance x_1 for FSPM due to normal force over linearly distributed source. The value of p shows a sharp increase for FSPM as x_1 increases for time $t = 0.01$ and 0.05.

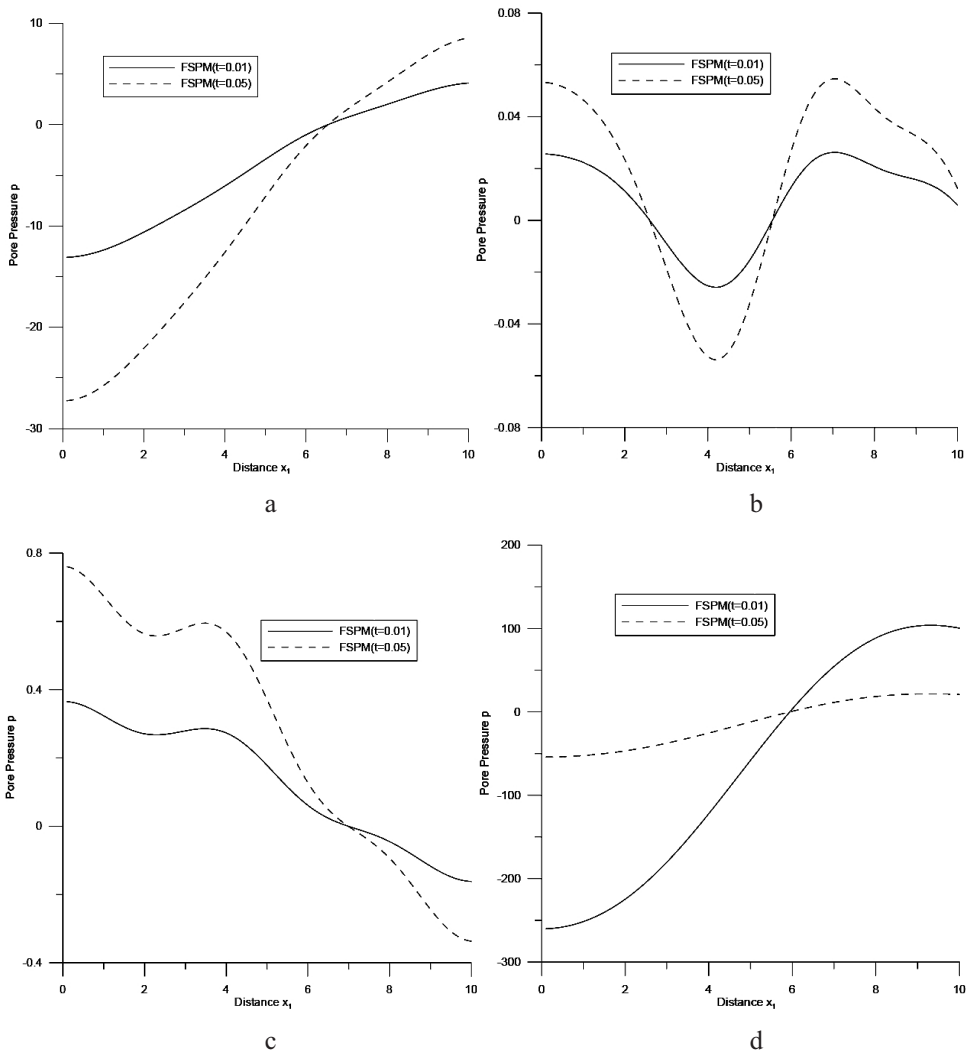

Fig. 9. Variation of pore pressure p with distance x_1 due to concentrated normal force (a), concentrated tangential force (b), concentrated pressure source (c), and thermal source (d).

Figure 9b shows the variation of pore pressure p w.r.t distance x_1 for FSPM due to tangential force over linearly distributed source. The value of p first decreases in the range $0 \le x_1 \le 4.2$ and then starts increasing for different values of time.

Figure 9c shows the variation of pore pressure p w.r.t distance x_1 for FSPM due to pressure source over linearly distributed source. The value of p starts decreasing as x_1 increases for different values of time.

Figure 9d shows the variation of pore pressure p w.r.t distance x_1 for FSPM due to thermal source over linearly distributed source. The value of p starts increasing as x_1 increases for both values of time.

Figure 10a shows the variation of temperature T w.r.t distance x_1 for FSPM and EPM due to normal force over linearly distributed source. The value of T first decreases and then oscillates for FSPM as x_1 increases for both value of time whereas for EPM it remain close to zero for both values of time.

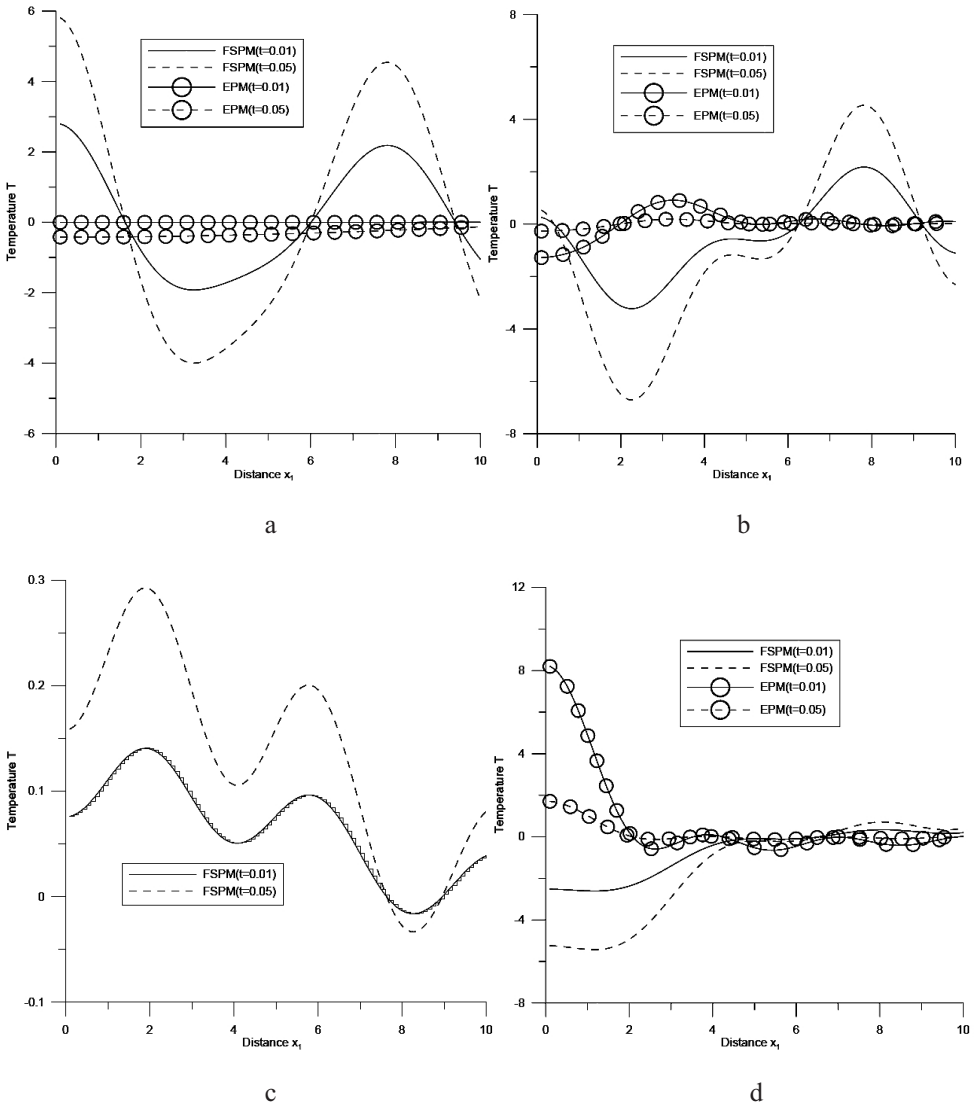

Fig. 10. Variation of temperature T with distance x_1 due to concentrated normal force (a), concentrated tangential force (b), concentrated pressure source (c), and thermal source (d).

Figure 10b shows the variation of temperature T w.r.t distance x_1 for FSPM and EPM due to tangential force over linearly distributed source. The value of T oscillates for FSPM and for EPM it remains close to zero in oscillatory manner as x_1 increases for different values of time.

Figure 10c shows the variation of temperature T w.r.t distance x_1 for FSPM due to pressure source over linearly distributed source. The value of T first increases and then starts decreasing for FSPM as x_1 increases for the time $t = 0.01$ and 0.05.

Figure 10d shows the variation of temperature T w.r.t distance x_1 for FSPM and EPM due to thermal source over linearly distributed source. The value of T first shows a small increase and then oscillates for FSPM whereas for EPM value of T first decreases in the range $0 \le x_1 \le 2.8$ and then becomes linear as x_1 increases for different values of time.

Conclusions. The components of displacement, stress, pore pressure and temperature change are obtained due to the various sources by using the Laplace and Fourier techniques. The values of the components of displacement, stress, pore pressure and temperature are close to each other due to CS, UDS and LDS. Near the application of the source, the porosity effect decreases the values of σ_{33} for normal force, pressure source and thermal source where as it decreases the values of p for normal force and tangential force but increases the values for thermal source.

Р е з ю м е

Досліджено двовимірну задачу щодо виникнення збурень від механічних і термічних джерел в однорідному теплопровідному пористо-пружному середовищі. При розв'язанні цієї задачі використовували перетворення Лапласа і Фур'є. Для ілюстрації перспективності даного підходу розглянуто різні випадки з точковими і розподіленими джерелами. За допомогою методики числової інверсії виконано перетворення компонент переміщень, напружень, тиску в порах і температурних флуктуацій. Вплив пористості на вказані параметри представлено у вигляді графіків. Розглянуто деякі спеціальні випадки, що мають практичний інтерес.

1. K. von Terzaghi, "Die Berechnug der Durchlässigkeit des Tones aus dem Verlauf der hydromechanischen Spannungserscheinungen," Sitzungsbericht der Akademie der Wissenschaften (Wien): Mathematisch-Naturwissenschaftlichen Klasse, **132**, 125–138 (1923).
2. K. von Terzaghi, *Erdbaumechanik auf bodenphysikalischer Grundlage*, Franz Deuticke, Leipzig–Wien (1925), p. 399.
3. M. A. Biot, "General theory of three dimensional consolidation," *J. Appl. Phys.*, **12**, No. 2, 155–161 (1941).
4. M. A. Biot, "Theory of propagation of elastic waves in fluid saturated porous solid. I. Low frequency range," *J. Acoust. Soc. Am.*, **28**, 168–178 (1956).
5. M. A. Biot, "Theory of propagation of elastic waves in fluid saturated porous solid. II. Higher frequency range," *J. Acousti. Soc. Am.*, **28**, 179–191 (1956).
6. M. A. Biot, "Mechanics of deformation and acoustic propagation in porous media," *J. Appl. Phys.*, **33**, No. 4, 1482–1498 (1962).
7. R. Kumar and B. S. Hundal, "The wave propagation in a fluid saturated incompressible porous medium," *Indian J. Pure Appl. Math*., **34**, No. 4, 651–665 (2003).
8. B. Bai and T. Li, "Solution for cylindrical cavety in saturated thermoporoelastic medium," *Acta Mech. Solida Sinica*, **22**, No. 1, 85–92 (2009).

9. B. Bai, "Response of saturated porous media subjected to local thermal loading on the surface of semi-space," *Acta Mech. Sinica*, **22**, 54–61 (2006).
10. B. Bai, "Thermal response of saturated porous spherical body containing a cavity under several boundary conditions," *J. Therm. Stress.*, **36**, No. 11, 1217–1232 (2013).
11. B. Bai, "Fluctuation responses of porous media subjected to cyclic thermal loading," *Comp. Geotech.*, **33**, 396–403 (2006).
12. S. Kaushal, R. Kumar, and A. Miglani, "Responce of frequency domain in generalized thermoelasticity with two temperature," *J. Eng. Phys. Thermophys.*, **83**, No. 5, 1080–1088 (2010).
13. M. Jabbari and H. Dehbani, "An exact solution for classic coupled thermoelasticity in axisymmetric cylinder," *J. Solid Mech.*, **2**, No. 2, 129–143 (2010).
14. M. Jabbari and H. Dehbani, "An exact solution for quasi-static poro-thermoelasticity in spherical coordinate," *Iran. J. Mech. Eng.*, **12**, No. 1, 86–108 (2011).
15. I. Abbas, "Natural frequencies of a poroelastic hollow cylinder," *Acta Mech.*, **186**, No. 1, 229–237 (2006).
16. A. N. Abd-alla and I. Abbas, "A problem of generalized magnetothermo-elasticity for an infinitely long, perfectly conducting cylinder," *J. Therm. Stress.*, **25**, No. 11, 1009–1025 (2002).
17. T. He and L. Cao, "A problem of generalized magneto-thermoelastic thin slim strip subjected to a moving heat source," *Math. Comp. Model.*, **49**, 1710–1720 (2009).
18. I. Abbas, "Generalized magneto-thermoelasticity in a nonhomogeneous isotropic hollow cylinder using the finite element method," *Arch. Appl. Mech*., **79**, 41–50 (2009).
19. I. A. Abbas, A. N. Abd-alla, and M. I. A. Othman, "Generalized magneto-thermo-elasticity in a fiber-reinforced anisotropic half-space," *Int. J. Thermophys*., 32, 1071–1085 (2011).
20. I. A. Abbas, "Generalized magneto-thermoelastic interaction in a fiber-reinforced anisotropic hollow cylinder," *Int. J. Thermophys*., **33**, 567–579 (2012).
21. I. A. Abbas and A. M. Zenkour, "LS model on electro-magneto-thermoelastic response of an infinite functionally graded cylinder," *Compos. Struct.*, **96**, 89–96 (2013).
22. I. A. Abbas and S. M. Abo-Dahab, "On the numerical solution of thermal shock problem for generalized magneto-thermoelasticity for an infinitely long annular cylinder with variable thermal conductivity," *J. Comput. Theor. Nanosci.*, **11**, No. 3, 607–618 (2014).
23. I. A. Abbas, "Fractional order GN model on thermoelastic interaction in an infinite fibre-reinforced anisotropic plate containing a circular hole," *J. Comput. Theor. Nanosci.*, **11**, No. 2, 380–384 (2014).
24. I. A. Abbas, "A GN model for thermoelastic interaction in an unbounded fiber-reinforced anisotropic medium with a circular hole," Appl. Math. Lett., **26**, 232–239 (2013).
25. R. Kumar, V. Gupta, and I. A. Abbas, "Plane deformation due to thermal source in fractional order thermoelastic media," *J. Comput. Theor. Nanosci.*, **10**, No. 10, 2520–2525 (2013).
26. I. A. Abbas, R. Kumar, and V. Chawla, "Response of thermal source in a transversely isotropic thermoelastic half-space with mass diffusion by using a finite element method," *Chinese Phys. B*, **21**, No. 8, 084601-1–084601-7 (2012).

27. A. M. Zenkour and I. A. Abbas, "Magneto-thermoelastic response of an infinite functionally graded cylinder using the finite element model," *J. Vibr. Control*, **20**, No. 12, 1907–1919 (2014).

28. I. A. Abbas and R. Kumar, "Interaction due to a mechanical source in transversely isotropic micropolar media," *J. Vibr. Control*, **20**, No. 11, 1607–1621 (2014).

29. I. A. Abbas, "A GN model based upon two-temperature generalized thermoelastic theory in an unbounded medium with a spherical cavity," *Appl. Math. Comput.*, **245**, 108–115 (2014).

30. M. Jabbari and H. Dehbani, "An exact solution for classic coupled thermoporo-elasticity in cylinderical coordinate," *J. Solid Mech*., **1**, No. 4, 343–357 (2009).

31. R. Kumar and L. Rani, "Elastodynamic response of mechanical and thermal source in generalized thermoelastic half space with voids," *Mech. Mechanic. Eng.*, **9**, No. 2, 29–45 (2005).

Received 06. 11. 2014